Letter

Robust magnetism and phase transitions in ultrathin Na_2IrO_3 flakes

Deepak K. Roy and Mukul Kabir*

Department of Physics, Indian Institute of Science Education and Research, Pune 411008, India

(Received 24 April 2024; accepted 25 June 2024; published 11 July 2024)

Competing spin-orbit coupling, electron correlation, and structural distortion are crucial factors influencing the physics of oxides, including iridates. We investigate ultrathin chemically bonded layered Na_2IrO_3, which exhibits characteristics of a proximate quantum spin liquid in its bulk form. Employing first-principles calculations, we explore the interplay between Heisenberg and Kitaev interactions within the two-dimensional limit. Contrary to the conventional understanding of van der Waals materials, magnetism in ultrathin Na_2IrO_3 is reinforced in the two-dimensional limit. As the zigzag antiferromagnetic state stabilizes, it diverges further from the Kitaev spin-liquid state due to enhanced Heisenberg and off-diagonal exchange interactions. Furthermore, carrier doping can tune the electronic and magnetic states, resulting in combined Mott insulator-to-metal and antiferromagnetic-to-ferromagnetic transitions. These findings provide compelling insights into the magnetism of a two-dimensional realm in non-van der Waals correlated oxide flakes.

DOI: 10.1103/PhysRevB.110.L020403

Introduction. A quantum spin liquid (QSL) is an exotic state of matter where highly correlated spins evade a symmetry-breaking phase transition down to the lowest temperatures [1–3]. QSLs exhibit long-range entanglement, topological order, emergent gauge fields, and fractional excitations that attracted enormous attention in quantum condensed matter physics. The Kitaev QSL state is an exact solution to a model Hamiltonian with bond-specific $S = 1/2$ nearest-neighbor Ising interactions, $K_\gamma S_i^\gamma S_j^\gamma$, where γ denotes different bonds [4]. In this model, the spin fractionalizes into itinerant and localized Majorana fermions.

Realizing the Kitaev QSL state in real materials is challenging due to the existence of additional spin interactions, such as the Heisenberg exchange [5–9]. In this context, spin-orbit entangled pseudospins on a honeycomb lattice can generate a Kitaev interaction in the edge-shared octahedral Mott insulators. The interplay between correlation and spin-orbit coupling makes Ir^{4+} oxides and Ru^{3+} chloride the primary candidate materials for hosting Kitaev QSL state [10–17]. Among the iridates, Na_2IrO_3 has received considerable attention since it was envisioned for realizing Kitaev physics [5,6]. Due to the extended Ir-5*d* orbitals, iridates reside far away from the Mott-insulating limit, $U \gg W$, with U and W being the electron correlation and electronic bandwidth, respectively. Consequently, the delicate interplay between comparable U, W, and spin-orbit coupling λ_{Ir} becomes intriguing. Given the spin-orbital nature, the interactions between $j_{\mathrm{eff}} = 1/2$ pseudospins are highly anisotropic, and the conventional Heisenberg exchange is suppressed according to the Jackeli-Khaliullin (JK) mechanism [5,6]. However, distortions result in a reduction of the Kitaev interaction and an increase in the Heisenberg exchange [7,18]. Accordingly, at temperatures below 15 K, the bulk Na_2IrO_3 exhibits antiferromagnetic (AFM) ordering, forming a zigzag spin structure [10–13].

This Letter investigates ultrathin Na_2IrO_3 from two perspectives. First, we analyze the impact of dimensional reduction and carrier doping on proximate Kitaev physics. Second, we explore 2D magnetism with enhanced electron correlation and spin-orbit coupling, demonstrating layered oxides as a different platform. In both counts, we report intriguing results. The ordering temperature is enhanced in the 2D limit, contrary to typical van der Waals (vdW) magnets. Additionally, charge-doped flakes undergo a Mott insulator-to-metal transition alongside an intriguing magnetic phase transition. These results present an exciting opportunity for further exploration.

Results are obtained from density functional theory, implemented in the Vienna *ab initio* simulation package [19,20], and extended Heisenberg-Kitaev Hamiltonian. We account for the on-site Coulomb interaction, Hund's exchange, and spin-orbit coupling [21]. Comprehensive structural relaxations are conducted, and magnetic ordering temperatures are determined through Monte Carlo simulations utilizing the SpinW code [22]. Additional computational details are provided in the Supplemental Material [23–30].

Before exploring ultrathin flakes, it is imperative to reproduce experimental results for bulk Na_2IrO_3 and validate the methodology. Calculated structural, electronic, and magnetic properties agree well with various experimental techniques, including angle-resolved photoemission spectroscopy, optical conductivity, resonant inelastic x-ray scattering, and inelastic neutron scattering (Supplemental Material) [10–13,30–38]. The bulk exhibits a relativistic Mott-insulating state with filled $j_{\mathrm{eff}} = 3/2$ and half-filled $j_{\mathrm{eff}} = 1/2$ manifolds. Trigonal distortion Δ_t significantly influences the quantum state, yet the j_{eff} picture remains valid due to $\Delta_t < \lambda_{\mathrm{Ir}}$. However, this lifts the t_{2g} degeneracy, leading to partial quenching of orbital momentum in bulk Na_2IrO_3. The

*Contact author: mukul.kabir@iiserpune.ac.in

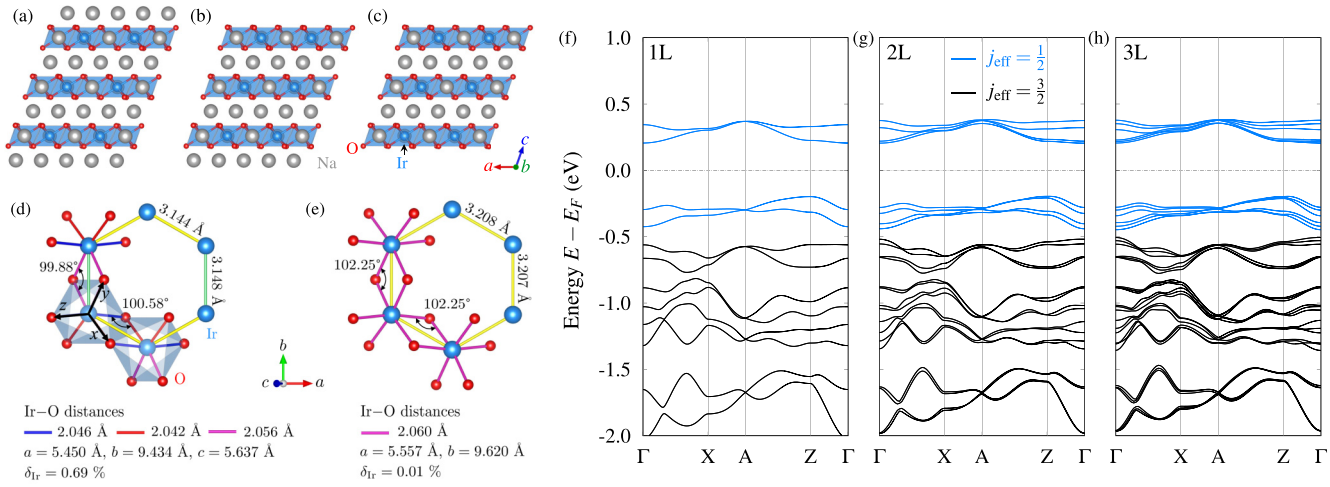

FIG. 1. (a)–(c) Different surface terminations are feasible for the ultrathin flakes, as illustrated for the three-layer (3L) Na_2IrO_3. The bulk structure comprises alternating layers of honeycomb $NaIr_2O_6$ and hexagonal Na_3 layers, making the flakes with and without the pure Na_3 termination equally plausible. Flakes where (a) both sides $[Na_3|\cdots|Na_3]$, (b) one side $[\otimes|\cdots|Na_3]$, and (c) none of the sides $[\otimes|\cdots|\otimes]$ are terminated with a Na_3 layer. Chemically passivated flakes are explored, though not depicted. Local structural details of the $NaIr_2O_6$ layer are represented in (d) for the bulk and (e) for the passivated monolayer, $[H\text{-}Na_3|NaIr_2O_6|Na_3\text{-}H]$. Na-atoms are omitted for clarity. Magnetic axes, $\{\alpha, \beta, \gamma\} = \{x, y, z\}$, are along three nearest-neighbor Ir-O bonds. Bonds of the same color represent equivalent Ir-O distances. Electronic band structures of passivated flakes are shown in (f)–(h), which remain spin-orbit coupled Mott insulators. Essential electronic structure parameters such as band gaps, bandwidths, and the electron correlation remain equivalent to those of bulk Na_2IrO_3.

distorted edge-shared octahedra disrupts the JK mechanism, triggering superexchange interactions. These interactions result in magnetic ordering below 15 K [10–12], driven by Heisenberg and off-diagonal interactions. Consistent with experiments [11–13], the ground state is a zigzag AFM configuration, energetically favored over FM, stripe, and Néel AFM states [30]. The calculated spin moment of 0.28 μ_B/Ir is smaller than anticipated for $j_{\text{eff}} = 1/2$ systems, aligning with trends observed in Ir^{4+} compounds [11,34–36]. Additionally, in agreement with experimental [37] and earlier theoretical results [39], μ_s and μ_o moments are weakly noncollinear, lying in the *ac* plane at an angle with the crystallographic ***a*** axis [30].

Ultrathin Na_2IrO_3 *flakes*. The bulk being a proximate QSL, ultrathin Na_2IrO_3 layers provide a fascinating opportunity to explore Kitaev and Heisenberg interactions in the 2D regime. The weaker Na-O bonds between the Na_3 and $NaIr_2O_6$ layers are cleaved, leading to flakes in the crystallographic *ab* plane [Figs. 1(a)–1(c)]. The exfoliation energy of 154 meV $Å^{-2}$ is comparable to that of previously exfoliated transition metal carbides [40–42]. The flakes, being either Na rich or Na deficient [43,44], are electron or hole doped at the surface, exerting an intriguing effect on their physical properties. Moreover, both neutral and charge-doped flakes demonstrate dynamic stability [30], as confirmed by phonon dispersions calculated using acoustic and rotational sum rules for the force constants [29]. Remarkably, such non-vdW flakes have recently been chemically exfoliated [45–47].

Charge-neutral flakes. Ultrathin layers terminated with Na_3 layers on both sides are charge neutralized through hydrogen passivation, $[H\text{-}Na_3|\cdots|Na_3\text{-}H]$. A Bader charge analysis demonstrates that the magnetic honeycomb $NaIr_2O_6$ sublayers exhibit the same charge distribution as the bulk [30]. The in-plane lattice parameters consistently increase with thickness reduction, being 2% longer in the monolayer compared to bulk [Figs. 1(d) and 1(e)] [30]. In the passivated monolayer, the Ir off-centering distortion δ_{Ir} substantially decreases from 0.69% in the bulk to 0.01%, while the trigonal distortion increases to $\theta_{\text{Ir}} \sim 95^\circ$ [30,48]. Independent of thickness, the electronic structure of the passivated flakes resembles that of the bulk, maintaining a relativistic Mott-insulating state with approximately 400 meV band gaps [Figs. 1(f)–1(h)]. The calculated octahedral splitting Δ_{OC} of 3.4 eV, effective correlation calculated from the upper and lower Hubbard bands of 0.6 eV, and bandwidths near the Fermi level, 160–250 meV, are consistent with bulk values [30].

Magnetism persists in passivated flakes with one to three $NaIr_2O_6$ sublayers, exhibiting a zigzag AFM state akin to the bulk (Table I). This is unexpected, as the bulk material orders only below 15 K. These findings demonstrate

TABLE I. Heisenberg exchanges J_1 and J_3, off-diagonal exchanges Γ and Γ', and Kitaev interaction K in meV were calculated for bulk Na_2IrO_3, charge-neutral monolayer, ML: $[H\text{-}Na_3|NaIr_2O_6|Na_3\text{-}H]$, and hole-doped h-ML: $[\otimes|NaIr_2O_6|\otimes]$. The calculated Néel temperature T_N for the bulk agrees excellently with experimental data [10–12], confirming the accuracy of the calculations. Remarkably, the zAFM magnetism strengthens in the charge-neutral monolayer, while hole doping triggers a magnetic phase transition.

		J_1	K	Γ	Γ'	J_3	$T_{\text{N/C}}$
Bulk	zAFM	7.22	−31.26	3.52	−3.24	3.56	18 K
ML	zAFM	6.96	−29.50	10.00	−5.96	6.14	32 K
h-ML	FM	−12.56	1.82	0.21	−0.50	−2.79	29 K

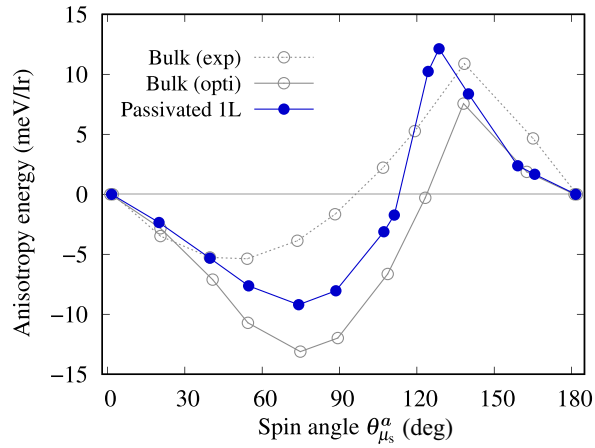

FIG. 2. The magnetic anisotropy energy in the crystallographic *ac* plane is illustrated as the spin moment rotates at an angle $\theta^{\boldsymbol{a}}_{\mu_s}$ relative to the $\boldsymbol{a}$ axis. These calculations employ the generalized gradient approximation (GGA) + SO + U_{Ir} + J_{H} approach within the zigzag AFM (zAFM) order. The energies are presented relative to the energy when the moment aligns along the $\boldsymbol{a}$ axis. The moments in the Mott-insulating zigzag AFM ground state are oriented at an angle to the $\boldsymbol{a}$ axis.

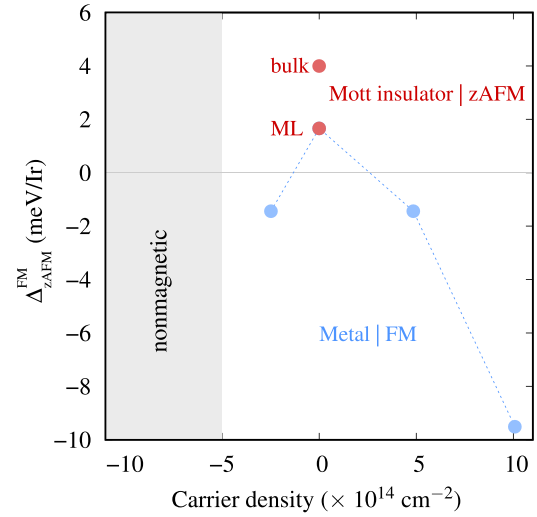

FIG. 3. The monolayer undergoes electronic and magnetic phase transitions in response to charge carriers. Variation in carrier density affects the relative energy $\Delta^{\mathrm{FM}}_{\mathrm{zAFM}}$ between the FM and the zigzag AFM phases. The density of states is available in the Supplemental Material [30].

that the conventional notion of diminishing ordering with decreasing thickness is not applicable in this context [49]. Additionally, the zigzag-ordered moments show a curious feature of not aligning with any of the crystallographic axes. In both monolayer and bulk, the Ir moments lie in the *ac* plane, forming angles of approximately 75° and 70°, respectively, with respect to the crystallographic $\boldsymbol{a}$ axis (Fig. 2). The spin and orbital moments in the bulk show weakly noncollinear behavior, with mutual angles below 10°, consistent with experimental [37] and theoretical findings [39]. This trend is maintained in the passivated monolayer, albeit with a higher degree of noncollinearity [30].

Charge-doped flakes. Surface termination influences charge carrier density, which can be further modulated through passivation [30]. The charge-doped flakes show reduced in-plane lattice parameters, particularly pronounced in hole-doped flakes. Other structural parameters such as Ir-O bonds, O-Ir-O, and Ir-O-Ir angles are also impacted. In flakes without the Na termination, Na-atoms from the adjacent $NaIr_2O_6$ magnetic layer undergo an out-of-plane displacement of 1.6 Å [30] indicative of Na volatility observed experimentally [43,50].

Charge doping induces intriguing electronic and magnetic phase transitions in ultrathin flakes of varying thicknesses. The metallic ferromagnetic state emerges in the monolayer, becoming more stable with increased carrier density (Fig. 3). However, no evidence of magnetism is observed in the highly electron-doped [Na_3|$NaIr_2O_6$|Na_3] monolayer. The moments correlate with carrier density, showing that μ_{o} decreases as density increases, particularly notable under hole doping, which also suppresses μ_{s} [30]. Consequently, effective spin-orbit coupling is reduced. At intermediate hole doping, the lower Hubbard band of j_{eff}-1/2 partially fills, resulting in a simultaneous decrease in both moments. In the presence of charge carriers, μ_{s} aligns with the c direction and becomes collinear with μ_{o}, differing from the bulk and neutral monolayer.

Magnetism in bilayer and trilayer is intricate, exhibiting a simultaneous presence of Mott-insulating AFM and metallic FM orders in distinct sublayers depending on carrier density [30]. Like the monolayer, extra electrons or holes induce a phase transition to a metallic FM state in the $NaIr_2O_6$ sublayer at the surface. For instance, the charge-neutral bilayer [H-Na_3|$\cdots$|Na_3-H] displays Mott-insulating behavior. However, a metallic [FM|FM] state emerges when both sides of the bilayer are terminated with or without the Na_3 layers, corresponding to electron and hole doping, respectively. Likewise, bilayers featuring a passivated Na_3-H layer on one side and carrier doping on the other (Fig. 4) stabilize in an AFM|FM phase. Consistent trends are observed in trilayers with different terminations [30]. Trilayers with and without Na_3 layers on both sides, representing electron-doped [Na_3|$\cdots$|Na_3] and hole-doped [$\otimes$|$\cdots$|$\otimes$], exhibit a [FM|AFM|FM] magnetic configuration.

Carrier doping occurs naturally in chemically exfoliated flakes, and multilayer flakes hold promise for diverse applications in spin-based devices, including magnetic tunnel junctions, magnetic sensors, spin filters, valves, and memory devices. However, it is important to note that devices integrating Na_2IrO_3 flakes will be limited to cryogenic temperatures. Nonetheless, the present results emphasize the possibility of naturally occurring spin devices and extend it to other materials capable of producing ultrathin layers that can maintain electronic and magnetic features at higher temperatures.

Extended Heisenberg-Kitaev model. We explore the microscopic details of magnetism using the extended Heisenberg-Kitaev (HK) Hamiltonian. Significant lattice distortion deviating from the ideal cubic octahedral environment renders a Heisenberg exchange, and a pure Kitaev Hamiltonian is

FIG. 4. Magnetic ordering in $NaIr_2O_6$ sublayers is dictated by the adjacent termination layer: the presence or absence ($\otimes$) of Na_3 layer, and a passivated Na_3-H layer. These terminations correspond to electron- or hole-doped and neutral magnetic $NaIr_2O_6$ sublayers, respectively. All possible terminations are studied, while the schematic illustrates a selection of them. The bilayer [H-Na_3|$\cdots$|Na_3] exhibits an [AFM|FM] state, while the [$\otimes$|$\cdots$|Na_3] bilayer demonstrates [FM|FM] ordering. Similarly, the [Na_3|$\cdots$|Na_3] trilayer displays a [FM|AFM|FM] configuration. The corresponding density of states is presented in the Supplemental Material [30].

inadequate to describe the physics. We consider a minimal HK Hamiltonian of the form [5–9]

$$\mathcal{H} = \sum_{\langle ij\rangle\in\alpha\beta(\gamma)} \left[J_1 \boldsymbol{S}_i\cdot\boldsymbol{S}_j + K S_i^\gamma S_j^\gamma + \Gamma\left(S_i^\alpha S_j^\beta + S_i^\beta S_j^\alpha\right) + \Gamma'\left(S_i^\beta S_j^\gamma + S_i^\gamma S_j^\beta + S_i^\gamma S_j^\alpha + S_i^\alpha S_j^\gamma\right)\right] + \sum_{\langle\langle\langle ij\rangle\rangle\rangle} J_3 \boldsymbol{S}_i\cdot\boldsymbol{S}_j,$$

where J_1 and J_3 are the first- and third-neighbor Heisenberg interactions, K is the Kitaev exchange, and Γ and Γ' are the symmetric off-diagonal exchange. $\boldsymbol{S}$ are the Ir^{4+} Kramers doublet pseudospin ($J_{\text{eff}} = 1/2$). $\{\alpha,\beta,\gamma\} = \{x,y,z\}$ are three nearest-neighbor bonds [Fig. 1(d)]. The non-Kitaev terms in the Hamiltonian induce a phase transition to a zigzag AFM state at 15 K [10–12]. Stronger J_1, J_3, Γ, and Γ' will drive the system further away from the QSL state. Therefore, exploring the evolution of competing exchange interactions from bulk Na_2IrO_3 to a single layer of spin-orbit coupled correlated electrons is intriguing.

The parameters of the HK Hamiltonian are determined using the four-state method (Table I) [26,27]. The Kitaev interaction in bulk Na_2IrO_3 is ferromagnetic and serves as the dominant energy scale, whereas the J_1 interaction is AFM and notably weaker, $|J_1| \ll K$. These results are consistent with *ab initio* calculations [9,27,51,52] and the same extracted from experimental data [8,53]. Furthermore, anisotropy in the magnetic susceptibility suggests the presence of a symmetric off-diagonal exchange [9,10], and fitting with experimental data indicates a non-negligible contribution when $K \gg |J_1|$. For bulk Na_2IrO_3, the calculated ratio of $\Gamma/(3J_1+K) \sim -0.37$ is consistent with previous predictions [9]. Stabilization of the zigzag AFM phase in honeycomb iridates is attributed to the third-neighbor Heisenberg exchange J_3, arising from an inversion center and finite *M-L-L-M* hopping in the system [18,52,53]. Similar to J_1, we find J_3 to be sizable and antiferromagnetic, with $J_3 \sim \Gamma$ and $J_3/J_1 \sim 0.5$. We computed Γ', which is ferromagnetic unlike Γ, but comparable in strength, $|\Gamma'| \sim |\Gamma|$. Hence, despite having a significant Kitaev interaction, bulk Na_2IrO_3 orders in the zigzag AFM phase due to considerable AFM Heisenberg exchanges J_1, J_3, as well as Γ and Γ' (Table I). The corresponding T_N is determined using Heisenberg-Kitaev Monte Carlo simulations with 10^4 spins and using parameters in Table I, yielding excellent agreement with experimental data [10–12].

The passivated monolayer maintains electronic equivalence to the bulk, yet specific structural alterations in 2D result in intriguing characteristics in the competing exchange interactions. Proceeding from the bulk to monolayer, the nature of interactions remains unchanged: FM for K and Γ' and AFM for J_1, J_3, and Γ (Table I). Furthermore, the magnitudes of Kitaev K and Heisenberg J_1 remain consistent. Conversely, the off-diagonal interactions Γ, Γ' and third-neighbor J_3 significantly increase, leading to $|K/J_1| \sim 4.2$, $J_3/J_1 \sim 0.9$, and $|\Gamma| > |J_3| \sim |\Gamma'|$. The origins of Γ and Γ' lie in competing metal-metal, ligand-assisted, and distortion-mediated hopping processes [18]. In Na_2IrO_3, where ligand-assisted hopping dominates [51], the concurrent increase in the Ir-O-Ir angle and trigonal distortion, as measured by the O-Ir-O angle [30], enhances Γ and Γ' in the monolayer. Consequently, the monolayer stabilizes the zigzag AFM phase, evident from a significant rise in T_N (Table I). The complex magnetism described here contrasts with that of non-Kitaev 2D magnets [49]. Analogously, a recent study on $RuCl_3$ has demonstrated an increase in off-diagonal exchanges due to lattice distortion [54].

A microscopic analysis of the magnetic phase transition reveals a fascinating picture in the hole-doped metallic flake (Table I). Contrary to the charge-neutral flakes and bulk material, the Heisenberg interactions become ferromagnetic and dominate over the antiferromagnetic Kitaev interaction, where $K \ll |J_1|$. Hole doping quenches the orbital moment, leading to a significant decrease in spin-orbit coupling [30]. Consequently, both the Kitaev and off-diagonal interactions experience substantial reductions, while the ferromagnetic J_1 and J_3, with $|K/J_1| \sim 0.14$ and $J_3/J_1 \sim 0.22$, govern the physics. These parameters correspond to a relatively higher Curie temperature T_C of 29 K.

The preceding discussion indicates that quantum electron confinement does not alter the Mott-insulating electronic or zigzag AFM magnetic state in neutral flakes. However, the 2D nature induces structural distortions, significantly affecting the microscopic magnetic interactions (Table I). Similarly, electronic and magnetic phase transitions in carrier-doped flakes are primarily driven by doping and lattice distortions.

Summary. We rigorously investigate magnetism in ultrathin flakes of correlated oxide Na_2IrO_3, considering its proximity to a QSL state in bulk. Surprisingly, magnetism persists even at the monolayer limit, with increased Heisenberg and off-diagonal exchange interactions, robustly reinforcing the zigzag AFM state. This enhanced magnetism in the 2D limit contrasts with the conventional trend observed in vdW magnets. Passivated flakes retain their Mott insulator characteristic, whereas naturally carrier-doped flakes undergo an insulator-to-metal transition. This electronic transition is accompanied by an antiferromagnetic-to-ferromagnetic transition. Hence, multilayer flakes show potential as low-temperature spin devices. These findings open avenues for

comprehending and harnessing 2D magnetism in non-vdW correlated oxides and underscore the importance of experimental assessment.

Acknowledgments. We thank Ashna Bajpai for initiating discussions following the exfoliation of Na_2IrO_3 flakes in her group, which led to the inception of this theoretical investigation. We gratefully acknowledge the support and resources provided by the PARAM Brahma Facility at IISER, Pune, under the National Supercomputing Mission. We acknowledge funding from NM-ICPS of the Department of Science and Technology, through the I-HUB Quantum Technology Foundation, Pune, India. D.K.R. acknowledges support from CSIR India through a research fellowship.

[1] L. Balents, Spin liquids in frustrated magnets, Nature (London) **464**, 199 (2010).

[2] J. Knolle and R. Moessner, A field guide to spin liquids, Annu. Rev. Condens. Matter Phys. **10**, 451 (2019).

[3] H. Takagi, T. Takayama, G. Jackeli, G. Khaliullin, and S. E. Nagler, Concept and realization of Kitaev quantum spin liquids, Nat. Rev. Phys. **1**, 264 (2019).

[4] A. Kitaev, Anyons in an exactly solved model and beyond, Ann. Phys. **321**, 2 (2006).

[5] G. Khaliullin, Orbital order and fluctuations in Mott insulators, Prog. Theor. Phys. Suppl. **160**, 155 (2005).

[6] G. Jackeli and G. Khaliullin, Mott insulators in the strong spin-orbit coupling limit: From Heisenberg to a quantum compass and Kitaev models, Phys. Rev. Lett. **102**, 017205 (2009).

[7] J. Chaloupka, G. Jackeli, and G. Khaliullin, Kitaev-Heisenberg model on a honeycomb lattice: Possible exotic phases in iridium oxides A_2IrO_3, Phys. Rev. Lett. **105**, 027204 (2010).

[8] J. Chaloupka, G. Jackeli, and G. Khaliullin, Zigzag magnetic order in the iridium oxide Na_2IrO_3, Phys. Rev. Lett. **110**, 097204 (2013).

[9] J. G. Rau, E. K.-H. Lee, and H.-Y. Kee, Generic spin model for the honeycomb iridates beyond the Kitaev limit, Phys. Rev. Lett. **112**, 077204 (2014).

[10] Y. Singh and P. Gegenwart, Antiferromagnetic Mott insulating state in single crystals of the honeycomb lattice material Na_2IrO_3, Phys. Rev. B **82**, 064412 (2010).

[11] F. Ye, S. Chi, H. Cao, B. C. Chakoumakos, J. A. Fernandez-Baca, R. Custelcean, T. F. Qi, O. B. Korneta, and G. Cao, Direct evidence of a zigzag spin-chain structure in the honeycomb lattice: A neutron and x-ray diffraction investigation of single-crystal Na_2IrO_3, Phys. Rev. B **85**, 180403(R) (2012).

[12] X. Liu, T. Berlijn, W.-G. Yin, W. Ku, A. Tsvelik, Y.-J. Kim, H. Gretarsson, Y. Singh, P. Gegenwart, and J. P. Hill, Long-range magnetic ordering in Na_2IrO_3, Phys. Rev. B **83**, 220403(R) (2011).

[13] S. K. Choi, R. Coldea, A. N. Kolmogorov, T. Lancaster, I. I. Mazin, S. J. Blundell, P. G. Radaelli, Y. Singh, P. Gegenwart, K. R. Choi, S.-W. Cheong, P. J. Baker, C. Stock, and J. Taylor, Spin waves and revised crystal structure of honeycomb iridate Na_2IrO_3, Phys. Rev. Lett. **108**, 127204 (2012).

[14] Y. Singh, S. Manni, J. Reuther, T. Berlijn, R. Thomale, W. Ku, S. Trebst, and P. Gegenwart, Relevance of the Heisenberg-Kitaev model for the honeycomb lattice iridates A_2IrO_3, Phys. Rev. Lett. **108**, 127203 (2012).

[15] H. B. Cao, A. Banerjee, J.-Q. Yan, C. A. Bridges, M. D. Lumsden, D. G. Mandrus, D. A. Tennant, B. C. Chakoumakos, and S. E. Nagler, Low-temperature crystal and magnetic structure of α-$RuCl_3$, Phys. Rev. B **93**, 134423 (2016).

[16] R. D. Johnson, S. C. Williams, A. A. Haghighirad, J. Singleton, V. Zapf, P. Manuel, I. I. Mazin, Y. Li, H. O. Jeschke, R. Valentí, and R. Coldea, Monoclinic crystal structure of α-$RuCl_3$ and the zigzag antiferromagnetic ground state, Phys. Rev. B **92**, 235119 (2015).

[17] K. Kitagawa, T. Takayama, Y. Matsumoto, A. Kato, R. Takano, Y. Kishimoto, S. Bette, R. Dinnebier, G. Jackeli, and H. Takagi, A spin–orbital-entangled quantum liquid on a honeycomb lattice, Nature (London) **554**, 341 (2018).

[18] S. M. Winter, A. A. Tsirlin, M. Daghofer, J. van den Brink, Y. Singh, P. Gegenwart, and R. Valentí, Models and materials for generalized Kitaev magnetism, J. Phys.: Condens. Matter **29**, 493002 (2017).

[19] G. Kresse and J. Hafner, *Ab initio* molecular dynamics for liquid metals, Phys. Rev. B **47**, 558 (1993).

[20] G. Kresse and J. Furthmüller, Efficient iterative schemes for *ab initio* total-energy calculations using a plane-wave basis set, Phys. Rev. B **54**, 11169 (1996).

[21] A. I. Liechtenstein, V. I. Anisimov, and J. Zaanen, Density-functional theory and strong interactions: Orbital ordering in Mott-Hubbard insulators, Phys. Rev. B **52**, R5467 (1995).

[22] S. Toth and B. Lake, Linear spin wave theory for single-Q incommensurate magnetic structures, J. Phys.: Condens. Matter **27**, 166002 (2015).

[23] P. E. Blöchl, Projector augmented-wave method, Phys. Rev. B **50**, 17953 (1994).

[24] J. P. Perdew, K. Burke, and M. Ernzerhof, Generalized gradient approximation made simple, Phys. Rev. Lett. **77**, 3865 (1996).

[25] H. J. Monkhorst and J. D. Pack, Special points for Brillouin-zone integrations, Phys. Rev. B **13**, 5188 (1976).

[26] H. J. Xiang, E. J. Kan, S.-H. Wei, M.-H. Whangbo, and X. G. Gong, Predicting the spin-lattice order of frustrated systems from first principles, Phys. Rev. B **84**, 224429 (2011).

[27] Y. S. Hou, J. H. Yang, H. J. Xiang, and X. G. Gong, First-principles study of the magnetic interactions in honeycomb Na_2IrO_3, Phys. Rev. B **98**, 094401 (2018).

[28] A. Togo and I. Tanaka, First principles phonon calculations in materials science, Scr. Mater. **108**, 1 (2015).

[29] F. Eriksson, E. Fransson, and P. Erhart, The HIPHIVE package for the extraction of high-order force constants by machine learning, Adv. Theor. Simul. **2**, 1800184 (2019).

[30] See Supplemental Material at http://link.aps.org/supplemental/10.1103/PhysRevB.110.L020403 for methodology details, bulk Na_2IrO_3 results compared with experimental findings, Bader analysis, phonon data, and structural, and electronic and magnetic parameters of the charge-neutral and charge-doped flakes, including band structures and density of states.

[31] R. Comin, G. Levy, B. Ludbrook, Z.-H. Zhu, C. N. Veenstra, J. A. Rosen, Y. Singh, P. Gegenwart, D. Stricker, J. N. Hancock, D. van der Marel, I. S. Elfimov, and A. Damascelli, Na_2IrO_3 as a novel relativistic Mott insulator with a 340-meV gap, Phys. Rev. Lett. **109**, 266406 (2012).

[32] H. Gretarsson, J. P. Clancy, X. Liu, J. P. Hill, E. Bozin, Y. Singh, S. Manni, P. Gegenwart, J. Kim, A. H. Said, D. Casa, T. Gog, M. H. Upton, H.-S. Kim, J. Yu, V. M. Katukuri, L. Hozoi, J. van den Brink, and Y.-J. Kim, Crystal-field splitting and correlation effect on the electronic structure of A_2IrO_3, Phys. Rev. Lett. **110**, 076402 (2013).

[33] C. H. Sohn, H.-S. Kim, T. F. Qi, D. W. Jeong, H. J. Park, H. K. Yoo, H. H. Kim, J.-Y. Kim, T. D. Kang, D.-Y. Cho, G. Cao, J. Yu, S. J. Moon, and T. W. Noh, Mixing between $J_{\rm eff} = \frac{1}{2}$ and $\frac{3}{2}$ orbitals in Na_2IrO_3: A spectroscopic and density functional calculation study, Phys. Rev. B **88**, 085125 (2013).

[34] M. Ge, T. F. Qi, O. B. Korneta, D. E. De Long, P. Schlottmann, W. P. Crummett, and G. Cao, Lattice-driven magnetoresistivity and metal-insulator transition in single-layered iridates, Phys. Rev. B **84**, 100402(R) (2011).

[35] M. A. Laguna-Marco, D. Haskel, N. Souza-Neto, J. C. Lang, V. V. Krishnamurthy, S. Chikara, G. Cao, and M. van Veenendaal, Orbital magnetism and spin-orbit effects in the electronic structure of $BaIrO_3$, Phys. Rev. Lett. **105**, 216407 (2010).

[36] A. Ruiz, A. Frano, N. P. Breznay, I. Kimchi, T. Helm, I. Oswald, J. Y. Chan, R. J. Birgeneau, Z. Islam, and J. G. Analytis, Correlated states in β-Li_2IrO_3 driven by applied magnetic fields, Nat. Commun. **8**, 961 (2017).

[37] S. Hwan Chun, J.-W. Kim, J. Kim, H. Zheng, C. C. Stoumpos, C. D. Malliakas, J. F. Mitchell, K. Mehlawat, Y. Singh, Y. Choi, T. Gog, A. Al-Zein, M. M. Sala, M. Krisch, J. Chaloupka, G. Jackeli, G. Khaliullin, and B. J. Kim, Direct evidence for dominant bond-directional interactions in a honeycomb lattice iridate Na_2IrO_3, Nat. Phys. **11**, 462 (2015).

[38] X. Xi, X. Bo, X. S. Xu, P. P. Kong, Z. Liu, X. G. Hong, C. Q. Jin, G. Cao, X. Wan, and G. L. Carr, Honeycomb lattice Na_2IrO_3 at high pressures: A robust spin-orbit Mott insulator, Phys. Rev. B **98**, 125117 (2018).

[39] K. Hu, F. Wang, and J. Feng, First-principles study of the magnetic structure of Na_2IrO_3, Phys. Rev. Lett. **115**, 167204 (2015).

[40] M. Naguib, O. Mashtalir, J. Carle, V. Presser, J. Lu, L. Hultman, Y. Gogotsi, and M. W. Barsoum, Two-dimensional transition metal carbides, ACS Nano **6**, 1322 (2012).

[41] M. Naguib, J. Halim, J. Lu, K. M. Cook, L. Hultman, Y. Gogotsi, and M. W. Barsoum, New two-dimensional niobium and vanadium carbides as promising materials for Li-ion batteries, J. Am. Chem. Soc. **135**, 15966 (2013).

[42] B. Anasori, Y. Xie, M. Beidaghi, J. Lu, B. C. Hosler, L. Hultman, P. R. C. Kent, Y. Gogotsi, and M. W. Barsoum, Two-dimensional, ordered, double transition metals carbides (MXenes), ACS Nano **9**, 9507 (2015).

[43] F. Lüpke, S. Manni, S. C. Erwin, I. I. Mazin, P. Gegenwart, and M. Wenderoth, Highly unconventional surface reconstruction of Na_2IrO_3 with persistent energy gap, Phys. Rev. B **91**, 041405(R) (2015).

[44] L. Moreschini, I. Lo Vecchio, N. P. Breznay, S. Moser, S. Ulstrup, R. Koch, J. Wirjo, C. Jozwiak, K. S. Kim, E. Rotenberg, A. Bostwick, J. G. Analytis, and A. Lanzara, Quasiparticles and charge transfer at the two surfaces of the honeycomb iridate Na_2IrO_3, Phys. Rev. B **96**, 161116(R) (2017).

[45] S. Homkar, B. Chand, S. S. Rajput, S. Gorantla, T. Das, R. Babar, S. Patil, R. Klingeler, S. Nair, M. Kabir, and A. Bajpai, Few-layer $SrRu_2O6$ nanosheets as non-van der Waals honeycomb antiferromagnets: Implications for two-dimensional spintronics, ACS Appl. Nano Mater. **4**, 9313 (2021).

[46] A. Puthirath Balan, S. Radhakrishnan, C. F. Woellner, S. K. Sinha, L. Deng, C. d. l. Reyes, B. M. Rao, M. Paulose, R. Neupane, A. Apte, V. Kochat, R. Vajtai, A. R. Harutyunyan, C.-W. Chu, G. Costin, D. S. Galvao, A. A. Martí, P. A. van Aken, O. K. Varghese, C. S. Tiwary *et al.*, Exfoliation of a non-van der Waals material from iron ore hematite, Nat. Nanotechnol. **13**, 602 (2018).

[47] R. Friedrich, M. Ghorbani-Asl, S. Curtarolo, and A. V. Krasheninnikov, Data-driven quest for two-dimensional non-van der Waals materials, Nano Lett. **22**, 989 (2022).

[48] M. A. Tovar-Olvera, P. Ruiz-Díaz, and M. Saubanère, Influence of local structural distortion on the magnetism of Na_2IrO_3 compounds, Phys. Rev. B **105**, 094413 (2022).

[49] M. Gibertini, M. Koperski, A. F. Morpurgo, and K. S. Novoselov, Magnetic 2D materials and heterostructures, Nat. Nanotechnol. **14**, 408 (2019).

[50] A. Vasdev, L. Yadav, S. Kamboj, K. Mehlawat, Y. Singh, and G. Sheet, Dynamic surface modification due to effusion of Na in Na_2IrO_3, J. Appl. Phys. **124**, 055102 (2018).

[51] S. M. Winter, Y. Li, H. O. Jeschke, and R. Valentí, Challenges in design of Kitaev materials: Magnetic interactions from competing energy scales, Phys. Rev. B **93**, 214431 (2016).

[52] L. Janssen, E. C. Andrade, and M. Vojta, Magnetization processes of zigzag states on the honeycomb lattice: Identifying spin models for α-$RuCl_3$ and Na_2IrO_3, Phys. Rev. B **96**, 064430 (2017).

[53] V. M. Katukuri, S. Nishimoto, V. Yushankhai, A. Stoyanova, H. Kandpal, S. Choi, R. Coldea, I. Rousochatzakis, L. Hozoi, and J. van den Brink, Kitaev interactions between $j = \frac{1}{2}$ moments in honeycomb Na_2IrO_3 are large and ferromagnetic: insights from *ab initio* quantum chemistry calculations, New J. Phys. **16**, 013056 (2014).

[54] B. Yang, Y. M. Goh, S. H. Sung, G. Ye, S. Biswas, D. A. S. Kaib, R. Dhakal, S. Yan, C. Li, S. Jiang, F. Chen, H. Lei, R. He, R. Valentí, S. M. Winter, R. Hovden, and A. W. Tsen, Magnetic anisotropy reversal driven by structural symmetry-breaking in monolayer α-$RuCl_3$, Nat. Mater. **22**, 50 (2023).